INTERNATIONAL JOURNAL OF CLIMATOLOGY
Int. J. Climatol. (2014)
Published online in Wiley Online Library
(wileyonlinelibrary.com) DOI: 10.1002/joc.3980

RMetS
Royal Meteorological Society

The impact of the Atlantic cold tongue on West African monsoon onset in regional model simulations for 1998–2002

Leonard M. Druyan[a,b]* and Matthew Fulakeza[a,b]

[a] *Center for Climate Systems Research, Columbia University, New York, NY, USA*
[b] *NASA/Goddard Institute for Space Studies, New York, NY, USA*

ABSTRACT: The Atlantic cold tongue (ACT) develops during spring and early summer near the Equator in the Eastern Atlantic Ocean and Gulf of Guinea. The hypothesis that the ACT accelerates the timing of West African monsoon (WAM) onset is tested by comparing two regional climate model (RM3) simulation ensembles. Observed sea surface temperatures (SST) that include the ACT are used to force a control ensemble. An idealized, warm SST perturbation is designed to represent lower boundary forcing without the ACT for the experiment ensemble. Summer simulations forced by observed SST and reanalysis boundary conditions for each of five consecutive years are compared to five parallel runs forced by SST with the warm perturbation. The article summarizes the sequence of events leading to the onset of the WAM in the Sahel region. The representation of WAM onset in RM3 simulations is examined and compared to Tropical Rainfall Measuring Mission (TRMM), Global Precipitation Climatology Project (GPCP) and reanalysis data. The study evaluates the sensitivity of WAM onset indicators to the presence of the ACT by analysing the differences between the two simulation ensembles. Results show that the timing of major rainfall events and therefore the WAM onset in the Sahel are not sensitive to the presence of the ACT. However, the warm SST perturbation does increase downstream rainfall rates over West Africa as a consequence of enhanced specific humidity and enhanced northward moisture flux in the lower troposphere.

KEY WORDS West African monsoon onset; Atlantic cold tongue; regional climate model

Received 5 August 2013; Revised 8 January 2014; Accepted 12 February 2014

1. Introduction

The West African monsoon (WAM) onset refers to the meridional migration of the intertropical discontinuity rainband from the Gulf of Guinea coast to the Sahel during late June or early July. The establishment of the spatial rainfall maximum near 10°N is related to increased continental sensible heating, which in turn initiates a surge in moisture convergence over the Sahel (Druyan *et al.*, 2010). The onset is usually preceded by a hiatus from heavy rain lasting several days. Thorncroft *et al.* (2011) describe the major stages in the annual West Africa (WA) precipitation cycle, based on ERA-I (European Centre for Medium Range Weather Forecasts interim reanalysis) data, 1989–2009: (1) an oceanic phase between November and mid-April when the rainband is broad with peak values just north of the Equator over the Atlantic near Africa, (2) a coastal phase between mid-April and the end of June when the rainfall peak is in the Gulf of Guinea coastal region around 4°N, (3) a transitional or 'break' phase during the first half of July when rainfall is rather light over WA and (4) a Sahelian phase between mid-July and September when the rainfall peak is established in the Sahelian region around 10°N. Earlier, Gu and Adler (2004) documented the break in WA rainfall during phase (3). The beginning of the Sahelian phase is referred to as the 'onset' in the literature (Sultan and Janicot, 2000; Hagos and Cook, 2007). These authors define onset as the day on which the running mean of precipitation at 10°N (Sahel) first exceeds the running mean at 5°N (Guinea coast). However, the data show that 5°N rainfall often remains heavy even after Sahel rainfall has reached summer levels. Sultan *et al.* (2005) suggest one motivation for studying the onset: sowing crops (of millet) near the monsoon onset date maximizes crop yields in WA countries.

Gallee *et al.* (2004) suggest that WAM onset occurring at the end of June is associated with the shift of the West African heat low (WAHL) from its Sahelian position (10–15°N) to its Saharan position (20–25°N). Lavaysse *et al.* (2009) study the characteristics of the WAHL migration, identifying it with the ECMWF ERA-40 reanalysis maximum of 925–700 mb thickness. They describe a northwestward displacement of the WAHL, from 19°–23°N to 22°–27°N, which they claim occurs approximately 5 days before the onset of monsoon rains during 1984–2001, with an average precipitation onset of 20 June.

Based on Weather Research and Forecasting (WRF) model's limited area simulations, Flaounas *et al.* (2012a) find that WAM onset timing in 2006 is not sensitive to the albedo of the Sahara, nor to the presence of mountains in North Africa, nor to the timing of the sea surface

* Correspondence to: Leonard M. Druyan, Center for Climate Systems Research, Columbia University, 2880 Broadway, New York, NY 10027, USA. E-mail: ld12@columbia.edu.

temperature (SST) cold tongue, which develops during late spring near the Equator in the Eastern Atlantic Ocean and Gulf of Guinea. However, shifting the large-scale boundary conditions forcing the WRF 2006 simulation forward and backward by 15 days has a clear impact on the timing of the WAM onset (Flaounas *et al.*, 2012a). This shifting modifies the timing of WAHL movements and of synoptic scale dry-air occurrences over the Sahel. Flaounas *et al.* (2012b) provide additional evidence of the role of lateral boundary forcing in triggering WAM onset timing. They deduce from atmospheric global climate model experiments and observations (1989–2008) that WAM onset timing is triggered by Rossby waves emanating from the Indian subcontinent. The initiation of convective activity over the Indian subcontinent north of 15°N at the time of the Indian monsoon onset results in the arrival of a westward propagating Rossby wave over North Africa 7–15 days later. After the passage of the wave, dry air intrusions weaken drastically. Hence, 20 days after the Indian monsoon onset, convection is released over the Sahel where thermodynamic conditions are more favourable. The studies of Flaounas *et al.* (2012a, 2012b) suggest that information sufficient to trigger onset timing is contained in the lateral boundary conditions (LBCs) driving regional atmospheric model simulations over WA.

Caniaux *et al.* (2011) find significant correlations between the dates of the intensification of the cold tongue (the mean date is June 10 with a standard deviation of 11 days) and WAM onset dates, based on an analysis of 27 years of data. Nguyen *et al.* (2011) study the timing of the annual onset of precipitation at the Gulf of Guinea coast, based primarily on Global Precipitation Climatology Project (GPCP) data for 1979–2009. In their analysis, the mean Sahelian onset occurs about 2 months after the coastal onset and 2 weeks after the end of the coastal phase. They conclude that both onsets are strongly controlled by the cold tongue development, although they deduce that the cold tongue is not the main factor triggering Sahelian onset. Thorncroft *et al.* (2011) also suggest that the seasonal evolution of WAM moisture fluxes, their convergence and associated rainfall are strongly affected by the Atlantic equatorial cold tongue. Okumura and Xie (2004) describe the results of two ensemble atmosphere–ocean global climate model (AOGCM) experiments that test the influence of the SST cold tongue on WAM onset. Their model's horizontal grid spacing is 2.8°. A control simulation uses prescribed SSTs with the full climatological seasonal cycle whereas the experiment uses equatorial Atlantic SSTs during boreal spring and summer that are modified to eliminate the cold tongue. Comparison of the resulting simulations implies that the presence of a fully developed cold tongue increases the northward gradient of air temperature, in turn leading to an acceleration of the southerly winds over the Gulf of Guinea. The intensity of this circulation increase suggests that the cold tongue contributes impetus to the northward advance of rainbands over WA. AOGCM deficiencies, especially its coarse horizontal resolution, suggest the prudence of testing their results using a higher resolution regional model.

Regional climate models (RCMs) could be useful for studying WAM onset. However, many RCMs overestimate precipitation prior to the actual onset, indicating too early a start of the rainy season by as much as a month (Jones *et al.*, 2011; Nikulin *et al.*, 2012; Druyan and Fulakeza 2013). RCM experiments to investigate mechanisms of WAM onset are best interpreted when actual SST forcing generates realistic onset timing. The study described in this article analyses simulations of climate evolution over WA generated by the RM3, a regional atmospheric model with previously documented skill in simulating the WAM (Druyan *et al.*, 2006, 2008, 2010; Druyan and Fulakeza, 2011). In particular, it evaluates the sensitivity of WAM onset indicators to the presence of the Atlantic cold tongue (ACT).

2. Model and experiments

The RM3 is a third generation version atmospheric model developed and run at the Center for Climate Systems Research (Columbia University) and the Goddard Institute for Space Studies (CCSR/GISS). The RM3 is integrated at 28 vertical sigma levels, with 5 mb top, on a horizontal grid with 0.44° spacing. Druyan *et al.* (2008) give the vertical coordinates for sigma surfaces. The domain (Figure 1), 49.5°S–49.5°N, 35°W–64°E, covers all of Africa, the Eastern Atlantic Ocean, the western Indian Ocean and southern Europe. RM3 uses the same land surface process model used in the GISS AOGCM (Rosenzweig and Abramopoulos 1997; Hansen *et al.*, 2002). The land surface model consists of two integrated parts, the soil and the canopy, and it conserves water and heat while simulating their vertical fluxes. The RM3-modelled soil is divided into six layers to a depth of 3.5 m, and the model distinguishes between five textures of soil. The canopy, modelled as a separate layer located above the soil, is responsible for the interception of precipitation, evaporation of accumulated water and removal of soil water through transpiration.

The RM3 uses the Del Genio and Yao (1993) moist convection parameterization and the Del Genio *et al.* (1996) scheme for the effects of cloud liquid water. These are components originally developed for the GISS global climate model, which itself has been extensively applied to climate sensitivity studies (Hansen *et al.*, 2002) and used in the 4th assessment of the Intergovernmental Panel on Climate Change. The cloud liquid water scheme allows for life cycle effects in stratiform clouds and permits cloud optical properties to be determined interactively. Druyan *et al.* (2008) show that RM3-simulated condensation within deep convection over WA produces peak cumulus heating rates near 500 mb.

RM3 simulations are driven here by LBCs from National Center for Environmental Prediction reanalysis 2 (NCPR2; Kanamitsu *et al.*, 2002). Externally specified LBCs are merged with RM3 computed values by weighting them with progressively decreasing weights inward within a buffer zone of six grid elements that completely

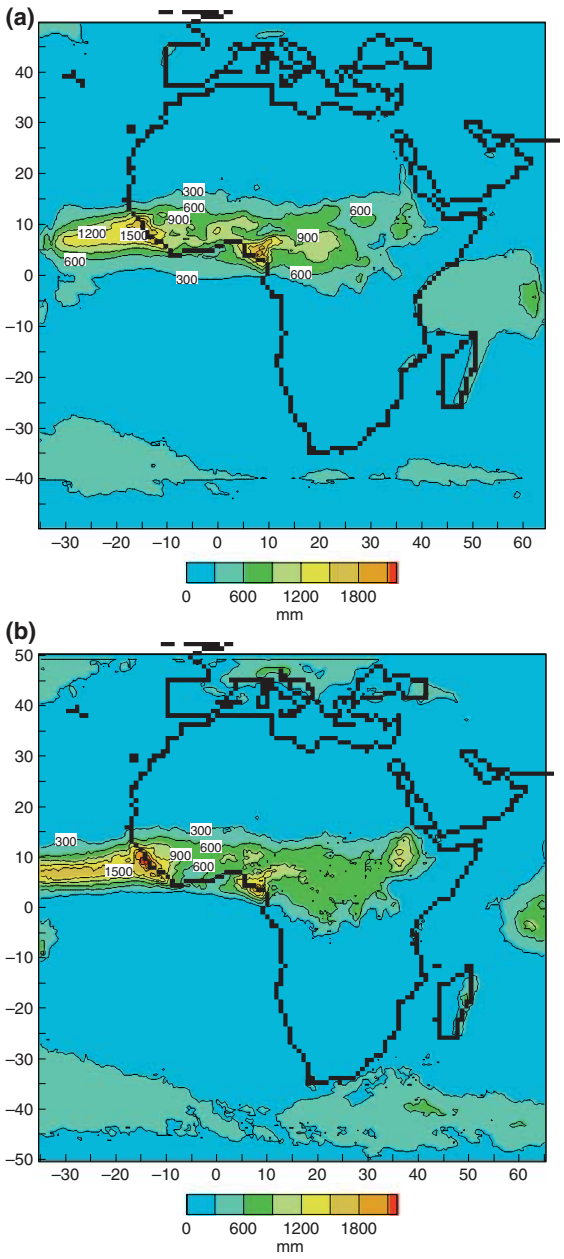

Figure 1. JJAS precipitation accumulations (mm) shown over the entire computational domain, averaged over 1998–2002: (a) RM3 control simulations, (b) TRMM (courtesy: NASA/GES/DISC; contour interval 300 mm).

surrounds the domain. Druyan and Fulakeza (2013) show that NCPR2 LBCs drive a more realistic RM3-simulated WAM onset than alternative ERA-I LBCs, at least for the years 1998–2002. Each of five RM3 control simulations is initialized from NCPR2 atmospheric conditions, SST and soil temperature and moisture at 00 UT on 30 November 1997, 1998, 1999, 2000, 2001, respectively. In addition, SST are interpolated from four times daily NCPR2, together with the LBCs, to form the RM3 lower ocean boundary conditions.

The study examines the modelled onset over WA during each year, 1998–2002. The year 1998 is the earliest for which Tropical Rainfall Measuring Mission (TRMM; Huffman *et al.*, 2007) data is available, so 1998 is selected as the first of 5 years for the current study. According to the rain gauge index given by Lélé and Lamb (2010), which is based on data between 11 and 18°N, west of 10°E, 1999 was the wettest year since the 1960s, experiencing a July–September departure of +133% of the JAS 1941–2000 mean. In 2002, the region registered a precipitation deficit of 37% of the 1941–2000 mean. The years 2000 and 2001 did not experience extreme precipitation anomalies, but 1998 was rainier than normal, with a departure of +79% of the base period mean. Thus, 1998–2002 represents a wide range of Sahel seasonal precipitation regimes. Comparisons between the control simulations and observations are given in Sections 3–6. A second set of RM3 simulation experiments is run just like the control, except for modifications to SST that effectively eliminate the ACT. The computation of the experimental SST and their impact on the evolving climate are given in Section 7. Section 8 summarizes results.

3. JJAS mean precipitation rates

Figure 1(a) and (b) respectively show RM3 control and TRMM (3B43 V7) June–September (JJAS) precipitation accumulations over the entire computational domain, averaged over 1998–2002. The southeastern North Atlantic Intertropical convergence zone (ITCZ) rainfall band is centred over 7°N. The RM3 ITCZ is disrupted on the west end by boundary effects, is somewhat too wide and underestimates the maximum by about 20%. This study focuses on the principal rainband over WA between 10°W and 10°E. While RM3 overestimates accumulations within the band 5–10°N, 10°W–10°E (north of the Gulf of Guinea coast), simulated precipitation accumulations over the Sahel (10–15°N) more closely match TRMM estimates. In addition, TRMM precipitation maxima along the coast near the Guinea Highlands and over the Cameroon coast and Highlands are reproduced realistically by RM3.

4. Sahel precipitation time series

RM3 simulations of precipitation are compared to TRMM (3B42 V7) estimates of daily precipitation accumulations interpolated to the model's 0.44° grid. Druyan *et al.* (2006) show a time correlation of 0.79 between TRMM daily estimates and the average of 34 colocated rain gauge daily accumulations near Niamey, Niger during July–September 2000, suggesting the reliability of TRMM. Figure 2 compares 5-day running means (5Drm) of 10–15°N, 10°E–10°W area averaged TRMM and RM3 rainfall during 3 June to 13 August, for each year, 1998–2002. This area is referred to as the 'Sahel' in subsequent discussions. The third curve on each graph in Figure 2 is discussed in Section 7. Each TRMM time series shows a range of Sahel precipitation rates of about

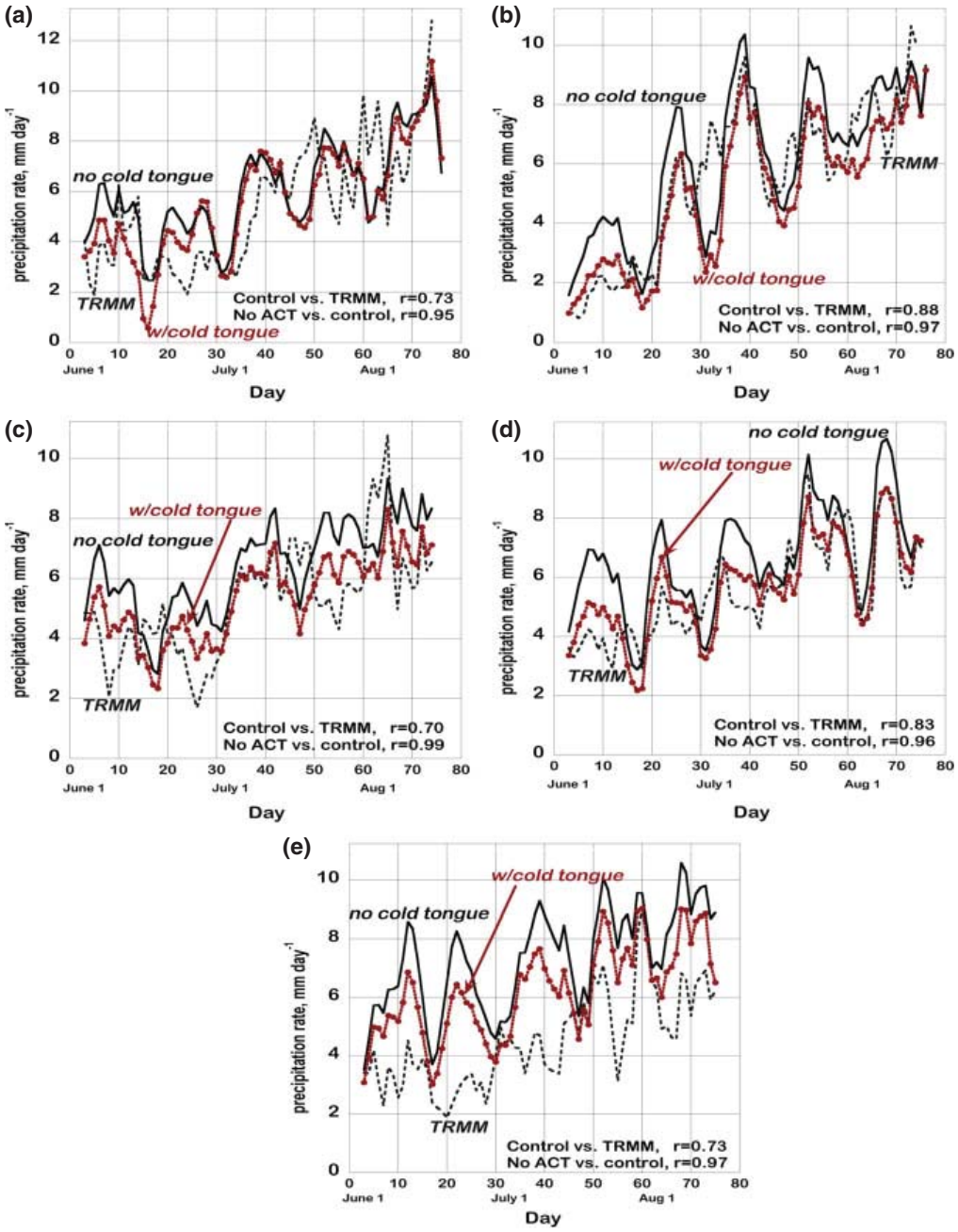

Figure 2. 5D running means of Sahel (10–15°N, 10°W–10°E) precipitation rates (mm day^{-1}): TRMM (dashed line; courtesy: NASA/GES/DISC), RM3 control (dotted line) and RM3 No ACT (solid line), 3 June to 13 August: (a) 1998, (b) 1999, (c) 2000, (d) 2001, (e) 2002.

2–4 mm day^{-1} during June, followed by a steady rise to about 6 mm day^{-1} either in late June or early July. The transition between these two states is one convenient representation of the monsoon precipitation onset.

Figure 3 compares the TRMM 5Drm time series to corresponding GPCP (Bolvin *et al.*, 2009) data. Vellinga *et al.* (2013) point out that TRMM uses precipitation radar measurements, which are not used in GPCP, making TRMM a valuable alternative data set. For the five 3 June to 13 August seasons considered, GPCP *versus* TRMM correlations of Sahel rainfall 5Drm range between $0.91 < r < 0.99$ and GPCP *versus* RM3 correlations of Sahel rainfall 5Drm range between $0.67 < r < 0.87$, not much different from the comparisons with TRMM. However, as GPCP is often rainier than TRMM, the 6 mm day^{-1} threshold is crossed by GPCP earlier in each of the 5 years. Moreover, although the threshold of 6 mm day^{-1} is consistent with the current analysis, other definitions found in the literature (Sultan and Janicot, 2000; Hagos and Cook, 2007; Vellinga *et al.*, 2013) yield different onset dates. It

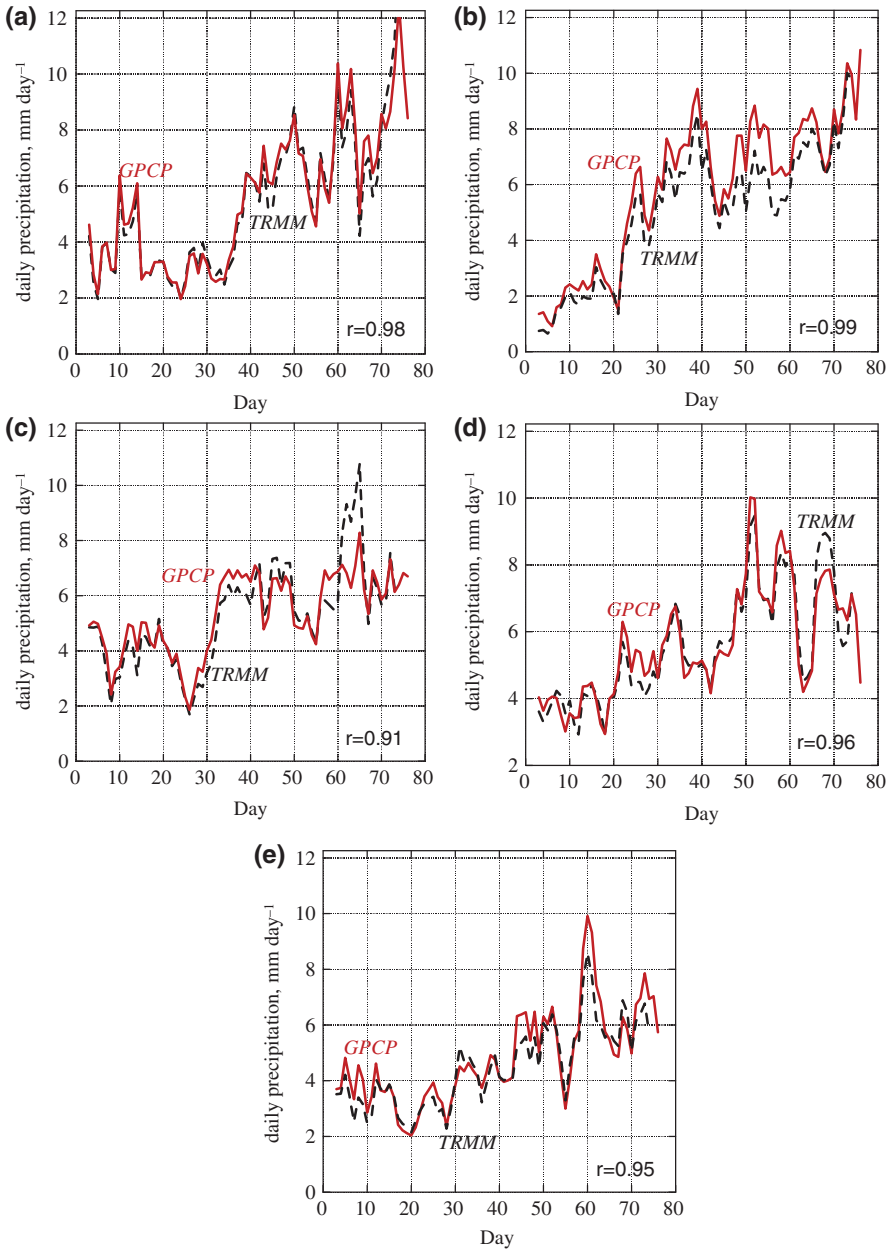

Figure 3. 5D running means of Sahel precipitation rates (mm day^{-1}): TRMM (dashed line; courtesy: NASA/GES/DISC) compared to GPCP (solid line; courtesy: NASA/GSFC/MAPL) (a) 1998, (b) 1999, (c) 2000, (d) 2001, (e) 2002.

will be shown below, however, that the impact of the ACT can be deduced unambiguously regardless of which onset definition is used.

The 5Drm of RM3-simulated Sahel daily rainfall for 3 June to 13 August 1998 *versus* TRMM data (Figure 2(a)) achieve a linear correlation of $r = 0.73$. Like TRMM, RM3 precipitation rates averaged about 4 mm day^{-1} during June and thereafter transition to higher values, which are maintained during July–August. In 1998, the transition to sustained levels of 5Drm above 6 mm day^{-1} occurs on 6 July 1998, some 3 days earlier than the corresponding onset detected by TRMM. In 1999, TRMM and RM3 5Drm (Figure 2(b)) are even better correlated than in 1998, with $r = 0.88$. Applying the 6 mm day^{-1} threshold indicates much earlier onset than in 1998. The RM3 5Drm Sahel precipitation rate is 5.9 mm day^{-1} on 25 June and it exceeds 6 mm day^{-1} on 26 June, although it drops during the subsequent week. TRMM values reach 6 mm day^{-1} on 25 June.

The correlation of the RM3 5Drm Sahel precipitation time series for 3 June to 13 August 2000 with TRMM is only $r = 0.70$. However, both time series show a similar, rather abrupt transition to higher values (Figure 2(c)), with RM3 5Drm first exceeding 6 mm day^{-1} on 5 July 2000,

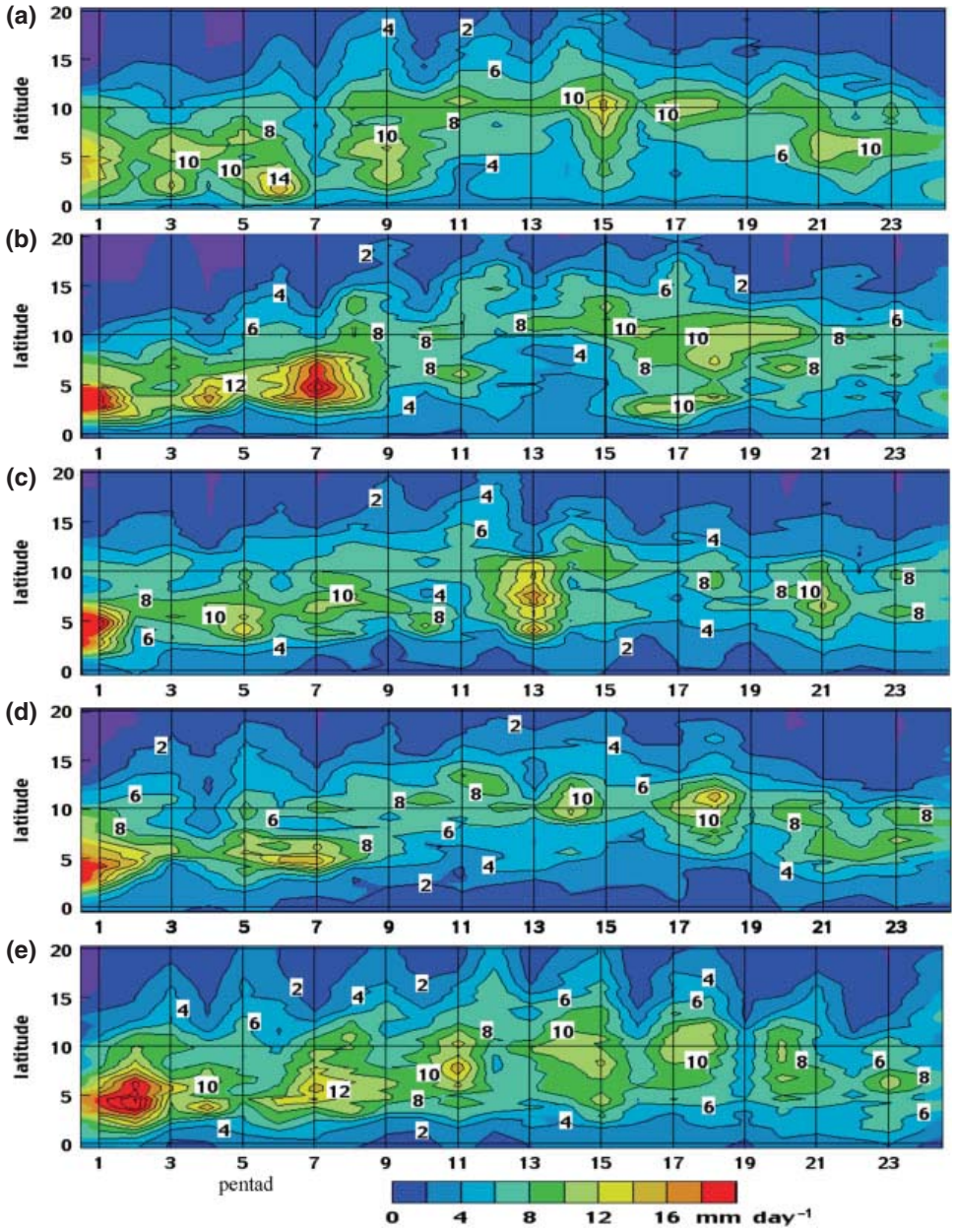

Figure 4. Hovmöller latitude *versus* pentad precipitation rates (mm day^{-1}) simulated for 1 June to 28 September by the RM3 control, averaged over 10°W–10°E: (a) 1998, (b) 1999, (c) 2000, (d) 2001, (e) 2002 (contour interval is 2 mm day^{-1}).

the same day as TRMM. TRMM and RM3 5Drm Sahel precipitation time series for 3 June to 13 August 2001 (Figure 2(d)) are correlated at $r = 0.83$. RM3 5Drm values reach 6 mm day^{-1} on 22 June 2001, before weakening. They next exceed that threshold on 5 July, 2 days after TRMM. TRMM and RM3 Sahel 5Drm rainfall time series for 3 June to 13 August 2002 (Figure 2(e)) are correlated at $r = 0.73$. TRMM does not break the 6 mm day threshold until 20 July. On the other hand, RM3 peaks are about 50% higher than TRMM during June–July, exceeding the threshold twice during June. This simulation initiated heavy rainfall north of 10°N much too early, as discussed below in more detail. In summary, the RM3 5Drm Sahel rainfall time series for five consecutive years are correlated with TRMM within a range of $0.70 < r < 0.88$. For three of the seasons, the RM3 onset is within 3 days of the TRMM onset. This is also true for 2001 if one ignores the premature episode of Sahel rain on 22 June.

5. Hovmöller time-latitude precipitation pentads

Tracing the meridional movement of pentad precipitation maxima on latitude-time Hovmöller distributions provides a more complete picture of onset and withdrawal.

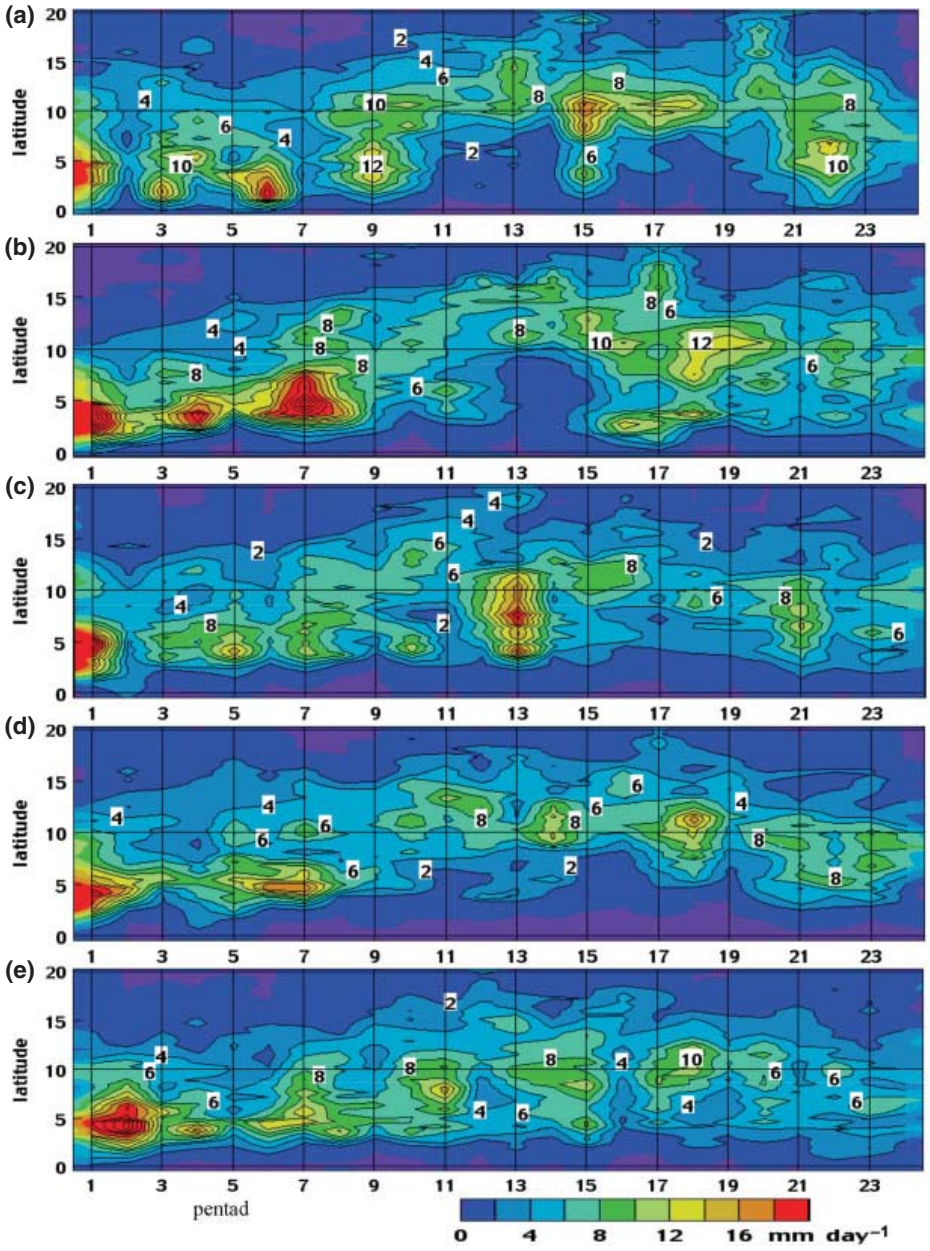

Figure 5. Hovmöller latitude *versus* pentad precipitation rates (mm day^{-1}), 1 June to28 September for TRMM (courtesy: NASA/GES/DISC), averaged over 10°W–10°E: (a) 1998, (b) 1999, (c) 2000, (d) 2001, (e) 2002 (contour interval is 2 mm day^{-1}).

Figures 4 and 5 respectively show RM3 and TRMM pentad precipitation for each of five 1 June to 28 September seasons, averaged between 10°W and 10°E at each latitude, 0°–20°N. Table 1 shows some statistics of comparison between the RM3 and TRMM Hovmöller distributions, including their high correlations. RM3 has a consistently positive bias owing to many more midrange values, but TRMM maxima are more extreme. TRMM data have higher standard deviations for four of the five seasons, with more very low and very high values. Overall, however, the RM3 simulations are a faithful representation of observed precipitation variability, demonstrated by correlation coefficients that exceed 0.90 for each year 1999–2002, and $r = 0.78$ for 1998. Thus, although the technical onset dates deduced from Figure 2 do not generally coincide, comparison of Figure 4 with Figure 5 shows that meridional movements of RM3 and TRMM rainbands are synchronized. As the RM3 simulation is forced with NCPR2 data, which are totally independent of TRMM, these high correlations suggest that both the RM3 and TRMM represent actual precipitation events. This is reinforced by the favourable comparisons between TRMM and GPCP discussed above.

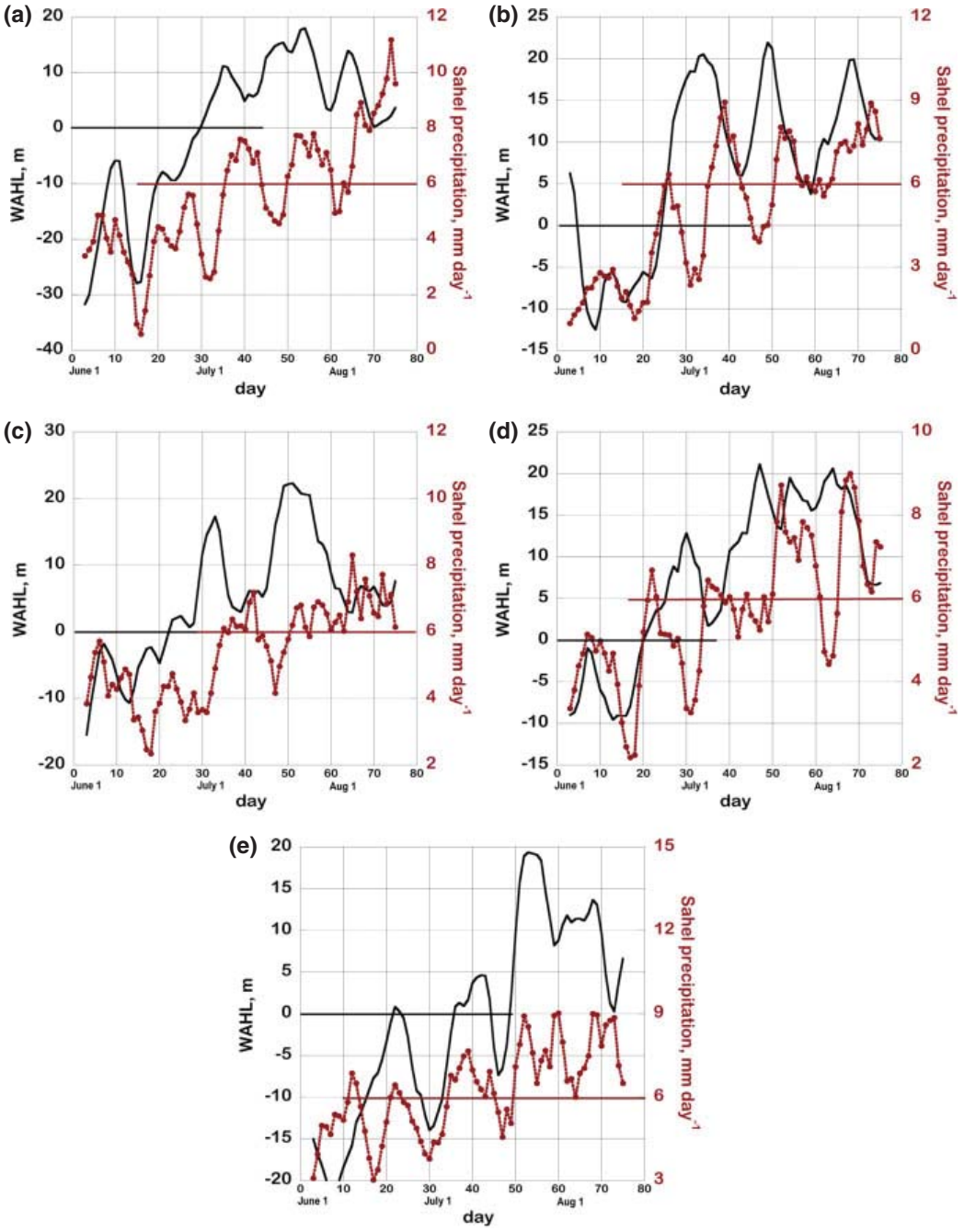

Figure 6. 5Drm of WAHL index (m; solid line) and Sahel precipitation rates simulated by RM3 control (mm day^{-1}; dotted line), 3 June to 13 August. The heavy horizontal lines indicate the respective onset thresholds for WAHL and Sahel precipitation: (a) 1998, (b) 1999, (c) 2000, (d) 2001, (e) 2002.

Figure 2(a) implies 1998 onset based on TRMM of 9 July and based on RM3 of 6 July. Consistent with this timing, pentad 7 (1–5 July) in Figures 4(a) and 5(a) distinctly shows a preonset break, followed by heavy rainfall at 10°N during pentad 8 (6–10 July). Figure 2(b) implies 1999 onset based on TRMM and RM3 of 25 June. Figures 4(b) and 5(b) indicate a relative minimum at pentad 5 (21–25 June) followed by an increase in rainfall along 10°N. Figure 2(c) implies 5 July 2000 onset based on TRMM and RM3. Figures 4(c) and 5(c) show a relative minimum during pentad 6 (26–30 June), but increases along and north of 10°N in pentads 7 and 8 (1–5 July; 6–10 July) are modest. The relative minimum of precipitation for pentad 4 (16–20 June) in 2001 (Figures 4(d), 5(d)) is followed by the onset of precipitation along 10°N, although TRMM Sahel rainfall that year (Figure 2(d))

Table 1. RM3 *versus* TRMM statistics of comparison for the pentad *versus* latitude precipitation rate distributions in Figures 4 and 5

Year	Correlation coefficients, RM3 *versus* TRMM	RM3 SD mm day^{-1}	TRMM SD mm day^{-1}	RM3 bias mm day^{-1}
1998	0.78	3.2	3.9	+1.0
1999	0.93	3.8	4.5	+0.4
2000	0.91	3.3	3.7	+0.6
2001	0.93	3.2	3.5	+0.8
2002	0.91	3.8	3.7	+1.7

exceeds the 6 mm day^{-1} threshold only on 3 July. Overall, RM3 precipitation excesses in 2002 create a wider rainband than observed by TRMM (Figures 4(e), 5(e)). Relatively heavy simulated rainfall spreads to the Sahel in early June. However, TRMM and RM3 both indicate a relative minimum for pentad 5 and large increases along 10°N for pentad 7. Despite the large rainfall bias of 2002, the RM3 distribution is highly correlated with TRMM. Note that, in each year, both TRMM and RM3 precipitation remain heavy near 5°N even after onset at 10°N.

6. The West African heat low (WAHL)

The climatological 'onset' of the WAHL, that is, when the WAHL moves towards its most western position, occurs around 20 June, 4 days on average before the WAM precipitation onset (Lavaysse *et al.*, 2009; Flaounas *et al.*, 2012a). Inspection of NCPR2 daily 925–700 mb thickness (ΔZ) distributions during June 1998 shows migration of the thickness maximum from 20°N, 2.5°E to 27.5°N, 5°W, roughly consistent with the Lavaysse *et al.* (2009) analysis of ERA-40.

Daily values of simulated ΔZ are examined to monitor the northwestward migration of the WAHL from the end of June and into July during each year, 1998–2002. The 5Drm WAHL index is plotted in Figure 6 for each season, computed as the difference between RM3 ΔZ at 27.5°N, 5°W minus ΔZ at 20°N, 2.5°E. This index becomes positive when the WAHL migrates to the northwest. RM3 time series of the WAHL index are closely correlated with corresponding NCPR2 data, so the following discussion refers to only RM3 results. To facilitate comparisons, the 5Drm RM3 Sahel rainfall for the corresponding season is plotted on each graph. Figure 6(a) shows that in 1998 the WAHL index first becomes positive on 30 June, some 6 days before the onset based on simulated Sahel rainfall, discussed above in connection with Figure 2(a). In 1999 (Figure 6(b)), the WAHL index becomes positive on 25 June, 1 day before the rainfall onset discussed above in connection with Figure 2(b). In 2000, WAHL becomes positive on 23 June (Figure 6(c)), 12 days before the rainfall onset. However, a big jump in the WAHL does occur on 29–30 June, only 6 days before the rainfall onset. In 2001, WAHL is first positive on 21 June (Figure 6(d)), a day before the earliest Sahel rainfall rates of at least 6 mm day^{-1}. The WAHL index during 2002 (Figure 6(e)) briefly becomes positive on 22–23 June and then again on 5 July. Simulated model precipitation for this case was excessive along 10°N throughout June. In summary, the RM3 WAHL index shows a similar time variation as the NCPR2 WAHL index. In four of the five seasons, the control simulated WAHL index becomes positive from 1 to 12 days before Sahel area mean rainfall passes the 6 mm day^{-1} threshold.

7. Atlantic cold tongue (ACT)

7.1. The ACT in observations

The ACT develops each spring just south of the Equator in the Eastern Atlantic Ocean. It typically intensifies during May and June. We consider whether the ACT affects WAM onset. Caniaux *et al.* (2011) define an index for the ACT that is positive wherever SST is cooler than 298 K within the area 5°S–5°N, 30°W–12°E. They define 'onset' of the cold tongue as the date on which the index is first positive over more than 40×10^4 km^2. Their onset dates for the cold tongue, based on their analysis of Reynolds *et al.* (2007) SST data, are computed as 24 June 1998, 14 June 1999, 12 June 2000, 7 June 2001 and 16 June 2002. Caniaux *et al.* (2011) explain that the intensification of the ACT increases the temperature gradient over the Gulf of Guinea coast, thereby accelerating the onshore near-surface circulation, which contributes to moisture transport into WA.

Table 2 summarizes the dates on which onset thresholds were reached in the RM3 control simulations and in Reynolds SST, which are used as the NCPR2 forcing data. For 1998–2001, the ACT reaches its threshold between 12 and 23 days before RM3 Sahel rainfall reaches the 6 mm day^{-1} threshold. In 2002, heavy Sahel precipitation already occurs some 4 days before the ACT matures. The date that the WAHL index becomes positive (computed from RM3 925–700 mb thickness) is fairly stable, ranging only between 21 and 30 June.

The sensitivity of the simulated seasonal evolution of the WAM to the ACT is tested by comparing the results of two ensemble simulations. Each ensemble of five simulations differs in the lower boundary conditions during 15 April to 30 September 1998, 1999, 2000, 2001 and 2002. The control ensemble, analysed above in Sections 3–6, uses NCPR2 SST (Reynolds *et al.*, 2007) supplied 4× per day, appropriate for the designated year, which include the ACT.

7.2. Sensitivity of WAM onset to the ACT

Five experimental simulations use modified equatorial SST that eliminate the ACT (hereafter 'No ACT'). Modifications of the SST are computed according to Okumura and Xie (2004) on Atlantic SST between 10°S and10°N according to the formula:

$$T_{ex} = T_{ob} + \left(T_{apr} - T_{ob}\right) \times \exp\left[-(LAT/10)^2\right]$$

Table 2. Dates of thresholds for simulated Sahel rainfall, simulated WAHL index and ACT in Reynolds SST data

Year/ indicator	Sahel rainfall rate first > 6 mm day^{-1}	WAHL index first > 0	First appearance of ACT[a]
1998	6 July	30 June	24 June
1999	26 June	25 June	14 June
2000	5 July	23 June	12 June
2001	22 June	21 June	7 June
2002	12 June	22 June	16 June

[a]According to Caniaux *et al.* (2011).

where T_{ex} is the SST for the experiment at any given time step and location, T_{ob} is the reanalysis SST at that time step and location, T_{apr} is reanalysis SST *on April 15* at the same location, exp is the exponential function, LAT is the latitude.

This function gives the largest modification at the Equator, wherever T_{apr} exceeds T_{ob} by a large amount. SST modifications become non-zero after 15 April, the approximate date when the ACT is first discernable.

To illustrate the modification of SST, Figure 7 shows the 5-year mean SST distributions for pentad 6 (26–30 June 1998–2002), close in time to most WAM onset dates and after the ACT is fully developed. Figure 7(a) shows the observed (control) SST, Figure 7(b) the No ACT SST and Figure 7(c) the SST perturbations. The analysed ACT appears along the Equator spanning 10°E–25°W, with a minimum value of about 298 K and a sharp positive gradient northward. The corresponding No ACT SST field is missing the northward gradient, which is replaced by a SST maximum of 302.6 K along 2°N. The modifications in SST represent imposed perturbations: $-1\,\mathrm{K} < \Delta\mathrm{SST} < 4\,\mathrm{K}$ (Figure 7(c)). This experiment represents a very idealized SST anomaly, as a completely missing ACT may never occur in nature. Accordingly, the lack of a fully interactive ocean that accounts for feedbacks allows us to consider a hypothetical scenario in which the ACT never develops during the first half of the summer.

The 5Drm time series of Sahel precipitation for the No ACT simulations for each of the five seasons are compared to TRMM and the control result in Figure 2. All of the No ACT time series are highly correlated with the corresponding control ($0.95 < r < 0.99$). The main difference is the somewhat rainier Sahel for the No ACT runs, although in 1998 this excess is mostly confined to June. As the experimental simulation forced by SST without the ACT produces generally higher precipitation rates than the control, the 6 mm day^{-1} threshold is crossed 1–4 days earlier. Given the near perfect correlations between the control and No ACT Sahel precipitation time series, reflecting the similar timing of major precipitation events, the choice of precipitation onset definition does not influence the assessment of impact.

The foregoing results are reinforced by comparisons of the latitude-time Hovmöller distributions of pentad precipitation. Table 1 indicates that control simulation distributions are fairly well-correlated with the corresponding

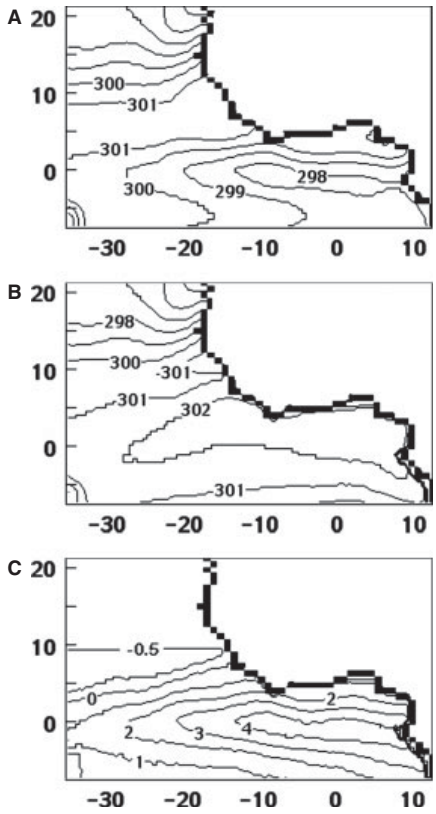

Figure 7. Pentad 6 (26–30 June) mean SST forcing (°K), averaged over 1998–2002: (a) control, (b) No ACT, (c) b minus a.

TRMM fields: $0.78 < r < 0.93$. In 1998 (Figure 8(a)), the removal of the ACT appears to have minimal effect on the pentad precipitation and no effect on the onset timing. Small impacts during June and early July include decreases in the experiment along 7°N and increases along 2°N. However, the preonset break still occurs during pentad 7 and the first heavy precipitation at 10°N still occurs in pentad 8. Pentad precipitation variability along 10°N is almost the same as in the control simulation. In both experiment and control, withdrawal occurs in pentad 22. A comparison of Figure 8(b) to Figure 4(b) shows that the time-latitude distribution of pentad precipitation in 1999 is likewise minimally affected by eliminating the ACT. Precipitation along 10°N in this simulation is slightly enhanced in June, as is the heavy rainfall of pentads 7 and 8. Mid-summer Sahel rainfall is also heavier. The onset is not delayed by the absence of the ACT and the timing of major precipitation events is unchanged. Pentad precipitation during 2000 is overall enhanced by eliminating the ACT and the rainband is widened. Compare Figure 8(c) to Figure 4(c). Thus, heavier rain reached 10°N already by the second pentad. There is no evidence that the imposed SST perturbations delayed or accelerated the northward migration of the centre of the rainband. In 2001, the removal of ACT SST forcing does not change the location of any of the precipitation maxima and does not affect the northward migration of the rainband. Compare Figure 8(d) to Figure 4(d). The most noticeable impact of

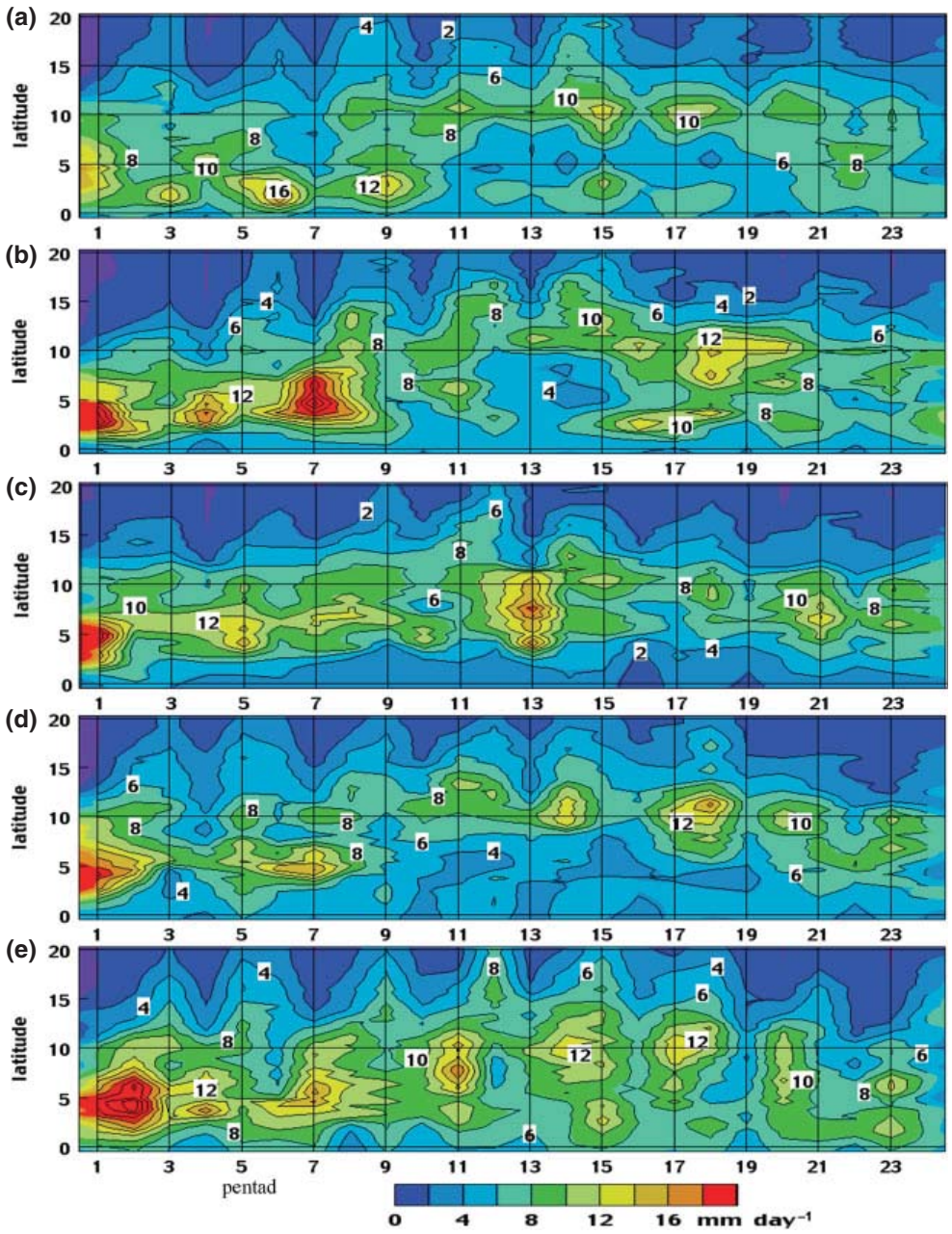

Figure 8. Hovmöller latitude *versus* pentad precipitation rates (mm day^{-1}) simulated for 1 June to 28 September by the RM3 No ACT, averaged over 10°W–10°E: (a) 1998, (b) 1999, (c) 2000, (d) 2001, (e) 2002 (contour interval is 2 mm day^{-1}).

No ACT is heavier precipitation, registered in many pentads at a number of latitudes. The observed dryness over 0–5°N is much better simulated with ACT forcing. For 2002, the No ACT simulation (Figure 8(e)) recreates the timing and latitudes of precipitation maxima of the control. However, maximum rates are increased in the experiment by some 20–30%. This simulation also increases Sahel rainfall rates and spreads moderate rates farther north. Moreover, the experiment widens the southern edge of the rainband, creating too much precipitation along the Gulf coast during middle to late summer.

In order to understand why removal of the ACT increases precipitation rates over WA, we examine No ACT minus control changes in meridional wind (v), specific humidity (q) and northward moisture transport (qv). Figure 9 shows these mean 1998–2002 changes for pentad 6 at 925 mb, which is representative of the moist monsoon layer. Removing the ACT imposes SST perturbations as high as 4 K (Figure 7(c)), creating a maximum of 302.6 K just north of the Equator (shown in Figure 7(b)). Figure 9(a) shows that the resulting diminished meridional SST gradients slow the 5-year mean v9 over the warmest

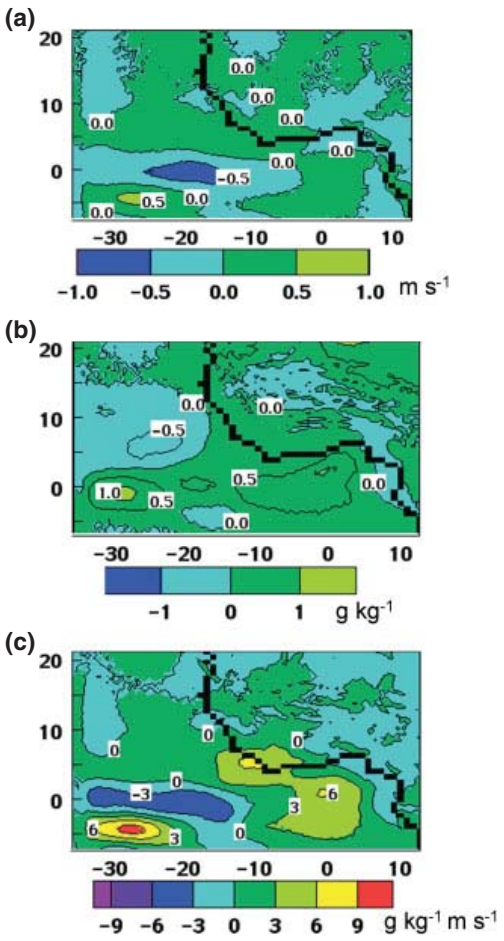

Figure 9. Pentad 6 (26–30 June) No ACT minus control differences, averaged over 1998–2002: (a) 925 mb meridional wind component, $m\,s^{-1}$, (b) 925 mb specific humidity, $g\,kg^{-1}$, (c) 925 mb meridional moisture flux, $g\,kg^{-1} \times m\,s^{-1}$.

perturbations. West of 10°W this circulation adjustment also weakens qv9 (Figure 9(c)). However, v9 for the No ACT simulations is not diminished at the Gulf of Guinea coast, perhaps as a feedback response to higher precipitation rates downstream. The 5-year mean q9 (Figure 9(b)) is slightly enhanced over the prescribed positive SST perturbations as well as over southern WA, increasing the moisture supply to the monsoon circulation. East of 10°W qv9 is enhanced despite small reductions in v9, whereas closer to 0° longitude, qv9 is additionally strengthened by increases in v9. In summary, elimination of the ACT boosts the 5-year mean qv9 (Figure 9(c)) over the Gulf of Guinea and the southwest coast of WA, transporting excess moisture into WA, leading to heavier rainfall.

The 5Drm WAHL index time series for the No ACT experiments are compared to the control results during the first half of the summer (not shown). Correlations between experiment and control WAHL index time series all exceed 0.92 and the WAHL onset date never changes by more than a single day. Thus, the presence or absence of the ACT has little effect on WAHL index time series.

8. Discussion and conclusion

The study examines the WAM onset for each of five seasons, 1998–2002. Many of the simulated precipitation features are shown to be realistic by their favourable comparison to TRMM and GPCP. Correlations between regional model and TRMM 5Drm Sahel precipitation rates, 3 June to 13 August, range from 0.70 to 0.88, so these completely independent systems somewhat validate each other. Corresponding GPCP time series of 5Drm Sahel precipitation rates are correlated with TRMM at $0.91 < r < 0.99$. Hovmöller distributions are shown of pentad WA precipitation *versus* latitudes 0–20°N for each season from TRMM observations and from corresponding regional model simulations forced by NCPR2. These model Hovmöller distributions are also well correlated with TRMM data, $0.78 < r < 0.93$, showing the same onset timing in the simulations as TRMM in four of the five seasons. Excessive precipitation simulated for 2002 implies a premature onset. The particular precipitation onset definition adapted for this study is illustrative for the comparisons, but does not affect the evaluation of the role of the ACT. Regional model simulations of the 925–700 mb thickness evolution during early summer recreate the observed relocation (in NCPR2 data) of the WAHL from 20°N, 2.5°E to 27.5°N, 5°W, usually occurring earlier than the precipitation onset.

The impact of the ACT on WAM onset is examined by comparing the control simulations forced by observed SST to parallel simulations with modified SST that eliminate the ACT. In nature, there is a continuous interaction between the atmosphere and the ocean surface that is not modelled in prescribed SST experiments. For example, a weaker meridional temperature gradient might in turn weaken wind speeds and subsequently weaken upwelling of cold water in a positive feedback cycle. The current experiments, however, test a hypothetical scenario for which the ACT is absent in order to evaluate its role in forcing atmospheric evolution. The idealized No ACT experiment provides insight into the impact of the ACT even though it simulates a scenario that may never occur in nature. Moreover, the limited sampling of 5 years does not assure that results can be generalized for longer periods. The study employs the same LBCs for control and experimental simulations, as did a previous WRF study of WAM onset. Undoubtedly, this constrains the evolution of the WAM in contrast to AOGCM simulations for which the entire global atmosphere is free to react to local SST anomalies (Okumura and Xie 2004). Accordingly, any feedback that SST anomalies in the Gulf of Guinea could conceivably have on the vertical distributions of conditions at the rather distant domain boundaries is not accounted for in the current experimental design.

Results imply that removing the ACT does not delay the northward migration of precipitation, nor does it change the date that the WAHL index becomes positive. The unambiguous impact of replacing the ACT with warmer SST is to increase rainfall rates downstream over WA throughout the summer. The timing of major rainfall events

is not affected. Higher rainfall rates are attributable to stronger meridional moisture flux towards the Sahel by the monsoon circulation. The stronger moisture flux, in turn, results from higher specific humidity above the prescribed warm SST perturbations.

This study, therefore, does not support the AOGCM results of Okumura and Xie (2004), which suggest that the ACT accelerates WAM onset timing. The finding here that the WAM onset is rather insensitive to the ACT is, however, consistent with WRF RCM results reported by Flaounas *et al.* (2012a). Both RCM studies use the same LBCs for driving the control and the changed SST simulations. If the onset is indeed triggered by signals embedded in the LBCs (Flaounas *et al.*, 2012a), such as Rossby waves propagating from India (Flaounas *et al.*, 2012b), then the RCM studies testing the impact of changed SST lack this differential triggering mechanism. We find that elimination of the ACT is insufficient to alter the evolution of the WAM brought about by a given set of LBCs. By way of contrast, in the empirical studies of Caniaux *et al.* (2011), Thorncroft *et al.* (2011) and Nguyen *et al.* (2011), each season has its unique global forcing that is presumed to lead to a particular onset sequence. Perhaps the correlations between ACT appearance and onset timing imply that the same global forcing that produces early (late) Sahel rainfall onsets also creates a near-surface circulation that causes early (late) development of the ACT.

Acknowledgements

This research was supported by US National Science Foundation Grant AGS-10000874 and the NASA Cooperative Agreement NNX11AR63A. TRMM data were acquired using the GES-DISC Interactive Online Visualization and Analysis Infrastructure (Giovanni), part of NASA's Goddard Earth Sciences (GES) Data and Information Services Center (DISC). GPCP data were obtained from NASA/GSFC/MAPL. NCEP/DOE reanalysis 2 data used in the study were obtained from the NOAA-ESRL Physical Sciences Division, Boulder CO online from www.esrl.noaa.gov/psd. The authors gratefully acknowledge the constructive suggestions of two anonymous reviewers.

References

Bolvin D, Adler R, Huffman G, Nelkin E, Poutiainen J. 2009. Comparison of GPCP monthly and daily precipitation estimates with high-latitude gauge observations. *J. Appl. Meteorol. Climatol.* **48**: 1843–1857.

Caniaux G, Giordani H, Redelsperger J, Guichard F, Key E, Wade M. 2011. Coupling between the Atlantic cold tongue and the West African monsoon in boreal spring and summer. *J. Geophys. Res.* **116**: C04003.

Del Genio A, Yao M-S. 1993. Efficient cumulus parameterization for long-term climate studies. The GISS scheme. In *Cumulus Parameterization*. American Meteorological Society Monograph Series, Vol. 24, Emanuel K, Raymond D (eds). American Meteorological Society: Boston, MA; 181–184.

Del Genio A, Yao M-S, Kovari W, Lo K-W. 1996. A prognostic cloud water parameterization for global climate models. *J. Clim.* **9**: 270–304.

Druyan L, Fulakeza M. 2011. The sensitivity of African easterly waves to eastern tropical Atlantic sea-surface temperatures. *Meteorol. Atmos. Phys.* **113**: 39–53.

Druyan L, Fulakeza M. 2013. Downscaling reanalysis over continental Africa with a regional model: NCEP versus ERA forcing. *Clim. Res.* **56**: 181–196, DOI: 10.3354/cr01152.

Druyan L, Fulakeza M, Lonergan P. 2006. Mesoscale analyses of West African summer climate: focus on wave disturbances. *Clim. Dyn.* **27**: 459–481.

Druyan L, Fulakeza M, Lonergan P. 2008. The impact of vertical resolution on regional model simulation of the West African summer monsoon. *Int. J. Climatol.* **28**: 1293–1314.

Druyan L, Feng J, Cook K, Xue Y, Fulakeza M, Hagos S, Abdourahamane K, Moufouma-Okia W, Rowell D, Vizy E, Seidou S. 2010. The WAMME regional model intercomparison study. *Clim. Dyn.* **35**: 175–192.

Flaounas E, Janicot S, Bastin S, Roca R. 2012a. The West African monsoon onset in 2006: sensitivity to surface albedo, orography, SST and synoptic scale dry-air intrusions using WRF. *Clim. Dyn.* **38**: 685–708.

Flaounas E, Janicot S, Bastin S, Roca R, Mohino E. 2012b. The role of the Indian monsoon onset in the West African monsoon onset: observations and AGCM nudged simulations. *Clim. Dyn.* **38**: 965–983.

Gallee H, Moufouma-Okia W, Bechtold P, Brasseur O, Dupays I, Marbaix P, Messager C, Ramel R, Lebel T. 2004. A high resolution simulation of a West African rainy season using a regional climate model. *J. Geophys. Res.* **109**: D05108, DOI: 10.1029/2003JD004020.

Gu G, Adler R. 2004. Seasonal evolution and variability associated with the West African monsoon system. *J. Clim.* **17**: 3364–3377.

Hagos S, Cook K. 2007. Dynamics of the West African monsoon jump. *J. Clim.* **20**: 5264–5284.

Hansen J, Sato M, Nazarenko L, Ruedy R, Lacis A, Koch D, Tegen I, Hall T, Shindell D, Santer B, Stone P, Novakov T, Thomason L, Wang R, Wang Y, Jacob D, Hollandsworth S, Bishop L, Logan J, Thompson A, Stolarski R, Lean J, Willson R, Levitus S, Antonov J, Rayner N, Parker D, Christy J. 2002. Climate forcings in Goddard Institute for Space Studies SI2000 simulations. *J. Geophys. Res.* **107**: 4347.

Huffman G, Bolvin D, Nelkin E, Wolff D, Adler R, Gu G, Hong Y, Bowman K, Stocker E. 2007. The TRMM multisatellite precipitation analysis (TMPA): quasi global, multiyear, combined-sensor precipitation estimates at fine scales. *J. Hydrometeorol.* **8**: 38–55.

Jones C, Giorgi F, Asrar G. 2011. The coordinated regional downscaling experiment: CORDEX. An international downscaling link to CMIP5. *CLIVAR Exchanges* **16**(2): 34–40.

Kanamitsu M, Ebisuzaki W, Woollen J, Yang S-K, Hnilo J, Fiorino M, Potter G. 2002. NCEP-DEO AMIP-II reanalysis (R-2). *Bull. Am. Meteorol. Soc.* **83**: 1631–1643.

Lavaysse C, Flamant C, Janicot S, Parker DJ, Lafore JP, Sultan B, Pelon J. 2009. Seasonal evolution of the West African heat low: a climatological perspective. *Clim. Dyn.* **33**: 313–330.

Lélé I, Lamb P. 2010. Variability of the intertropical front (ITF) and rainfall over the West African Sudan–Sahel zone. *J. Clim.* **23**: 3984–4004.

Nguyen H, Thorncroft C, Zhang C. 2011. Guinean coastal rainfall of the West African Monsoon. *Q. J. R. Meteorol. Soc.* **137**: 1828–1840, DOI: 10.1002/qj.867.

Nikulin G, Jones C, Giorgi F, Asrar G, Büchner M, Cerezo-Mota R, Christensen O, Déqué M, Fernandez J, Hänsler A, van Meijgaard E, Samuelsson P, Sylla M, Sushama L. 2012. Precipitation climatology in an ensemble of CORDEX-Africa regional climate simulations. *J. Clim.* **25**: 6057–6078.

Okumura Y, Xie SP. 2004. Interaction of the Atlantic equatorial cold tongue and the African monsoon. *J. Clim.* **17**: 3589–3602.

Reynolds R, Smith T, Liu C, Chelton D, Casey K, Shlax M. 2007. Daily high resolution blended analysis for sea surface temperatures. *J. Clim.* **20**: 5473–5496.

Rosenzweig C, Abramopoulos F. 1997. Land-surface model development for the GISS GCM. *J. Clim.* **10**: 2040–2054.

Sultan B, Janicot S. 2000. Abrupt shift of the ITCZ over West Africa and intra-seasonal variability. *Geophys. Res. Lett.* **27**: 3353–3356.

Sultan B, Baron C, Dingkuhn M, Sarr B, Janicot S. 2005. Agricultural impacts of large-scale variability of the West African monsoon. *Agr. Forest. Meteorol.* **128**: 93–110.

Thorncroft C, Nguyen H, Zhang C, Peyrillé P. 2011. Annual cycle of the West African monsoon: regional circulations and associated water vapour transport. *Q. J. R. Meteorol. Soc.* **137**: 129–147.

Vellinga M, Arribas A, Graham R. 2013. Seasonal forecasts for regional onset of the West African monsoon. *Clim. Dyn.* **40**: 3047–3070.

